International Journal of Radiation Oncology biology • physics

www.redjournal.org

Biology Contribution

White and Gray Matter Abnormalities After Cranial Radiation in Children and Mice

Brian J. Nieman, PhD,[*,§,‖] A. Elizabeth de Guzman,[*,§] Lisa M. Gazdzinski, PhD,[*] Jason P. Lerch, PhD,[†,§] M. Mallar Chakravarty, PhD,[¶,#] Jon Pipitone,[**] Douglas Strother, MD,[††,‡‡] Chris Fryer, MD,[§§,‖‖] Eric Bouffet, MD,[*,¶¶] Suzanne Laughlin, MD,[‡,##] Normand Laperriere, MD,[*,†††] Lily Riggs,[†] Jovanka Skocic,[†] and Donald J. Mabbott, PhD[†,¶¶]**

Departments of *Physiology & Experimental Medicine, [†]Neurosciences & Mental Health, and [‡]Diagnostic Imaging, Hospital for Sick Children, Toronto, Ontario, Canada; [§]Department of Medical Biophysics, University of Toronto, Toronto, Ontario, Canada; [‖]Ontario Institute for Cancer Research, Toronto, Ontario, Canada; [¶]Cerebral Imaging Centre, Douglas Mental Health University Institute, Montreal, Quebec, Canada; [#]Departments of Psychiatry and Biomedical Engineering, McGill University, Montreal, Quebec, Canada; **Kimel Family Translational Imaging Genetics Research Laboratory, Research Imaging Centre, Centre for Addiction and Mental Health, Toronto, Ontario, Canada; [††]Alberta Children's Hospital, Calgary, Alberta, Canada; [‡‡]Departments of Oncology and Pediatrics, University of Calgary, Calgary, Alberta, Canada; [§§]Division of Oncology/Hematology/BMT British Columbia Children's Hospital and British Columbia Women's Hospital and Health Centre, Vancouver, British Columbia, Canada; [‖‖]Department of Pediatrics, University of British Columbia, Vancouver, British Columbia, Canada; [¶¶]Department of Paediatrics, University of Toronto, Toronto, Ontario, Canada; [##]Department of Medical Imaging, University of Toronto, Toronto, Ontario, Canada; ***Department of Radiation Oncology, Princess Margaret Hospital/University Health Network, Toronto, Ontario, Canada; and [†††]Department of Radiation Oncology, University of Toronto, Toronto, Ontario, Canada

Received May 6, 2015, and in revised form Jul 27, 2015. Accepted for publication Jul 29, 2015.

Summary

We retrospectively evaluated brain anatomy in children treated with cranial radiation

Purpose: Pediatric patients treated with cranial radiation are at high risk of developing lasting cognitive impairments. We sought to identify anatomical changes in both gray matter (GM) and white matter (WM) in radiation-treated patients and in mice, in which the effect of radiation can be isolated from other factors, the time course of

Reprint requests to: Brian J. Nieman, PhD, Mouse Imaging Centre, Hospital for Sick Children, Toronto Centre for Phenogenomics, 25 Orde St, Toronto, Ontario, Canada M5T 3H7. Tel: (647) 837-5828; E-mail: brian.nieman@utoronto.ca

Conflict of interest: Normand Laperriere has received honoraria from Roche and Merck. All other authors report no relationships relevant to this report.

Supplementary material for this article can be found at www.redjournal.org.

Acknowledgments—The authors acknowledge funding support from the Canadian Institutes of Health Research, the Natural Sciences and Engineering Research Council of Canada, and the Ontario Institute for Cancer Research through funding provided by the government of Ontario.

Int J Radiation Oncol Biol Phys, Vol. 93, No. 4, pp. 882–891, 2015

http://dx.doi.org/10.1016/j.ijrobp.2015.07.2293

therapy and conducted corresponding experiments in mice. Radiation treatment resulted in decreased white matter volume and increased cortical thickness in both species. Decreasing hippocampal volume was observed in patients after radiation but not in mice, although decreased growth and volume were seen in the mouse olfactory bulb. Results highlight the causative role of radiation therapy in impaired brain development and support investigation using a mouse model.

anatomical change can be established, and the effect of treatment age can be more fully characterized. Anatomical results were compared between species.

Methods and Materials: Patients were imaged with T_1-weighted magnetic resonance imaging (MRI) after radiation treatment. Nineteen radiation-treated patients were divided into groups of 7 years of age and younger (7−) and 8 years and older (8+) and were compared to 41 controls. C57BL6 mice were treated with radiation (n = 52) or sham treated (n = 52) between postnatal days 16 and 36 and then assessed with in vivo and/or ex vivo MRI. In both cases, measurements of WM and GM volume, cortical thickness, area and volume, and hippocampal volume were compared between groups.

Results: WM volume was significantly decreased following treatment in 7− and 8+ treatment groups. GM volume was unchanged overall, but cortical thickness was slightly increased in the 7− group. Results in mice mostly mirrored these changes and provided a time course of change, showing early volume loss and normal growth. Hippocampal volume showed a decreasing trend with age in patients, an effect not observed in the mouse hippocampus but present in the olfactory bulb.

Conclusions: Changes in mice treated with cranial radiation are similar to those in humans, including significant WM and GM alterations. Because mice did not receive any other treatment, the similarity across species supports the expectation that radiation is causative and suggests mice provide a representative model for studying impaired brain development after cranial radiation and testing novel treatments.

Introduction

Cranial radiation therapy (CRT) is an integral component of treatments for brain tumors and some high-risk forms of leukemia but is directly associated with late effects (1-3), which manifest years after treatment as cognitive, endocrine, or other dysfunctions (4, 5). Increased radiation dose is a significant risk factor for decreased intelligence quotient (IQ), reduced academic performance, and impairments in measurements of processing speed, memory, and executive function (6-9). Magnetic resonance imaging (MRI) measurements have identified reduced white matter (WM) volume, altered WM structure, and possible changes in hippocampal volume due to CRT (10-12). These measurements correlate with behavioral outcomes (12-15), suggesting an intuitive link between normal brain development and proper brain function. Understanding, preventing, and treating late effects are important research priorities (9, 16).

The mouse provides a controlled experimental model with which to characterize CRT effects that eliminates some of the challenges inherent in clinical studies. The mouse can be treated with CRT exclusive of other possible treatments or cancer effects, and outcome can be assessed over relatively short time periods (weeks to months instead of years to decades). Radiation treatment in mice also results in behavioral abnormalities, including impaired learning and memory that has been associated with reduced hippocampal neurogenesis (17-19). As may be expected (20, 21), anatomical changes through development are also present (22) with a dependence on age, dose, and sex (23), reminiscent of known risk factors in human patients (9, 24). Provided it is representative of the effects seen in patients, the mouse model will enable efficient study of late effect mechanisms and treatments to mitigate them.

Our purpose in this study was to perform a side-by-side evaluation of radiation-induced neuroanatomical changes in humans and mice. First, we expected this would allow an expanded evaluation of brain structure changes in patients, confirming expectations in WM and expanding to assess gray matter (GM) as well, particularly the cortex and hippocampus. Second, we wished to determine the extent to which phenotypes in mice mirrored these findings. This allowed isolation of the CRT effects from other clinical and treatment factors, provided additional insight into the possible time course of changes seen in patients, and permitted evaluation of the mouse model.

Methods and Materials

Human data

The data set included 144 T_1-weighted MRI scans collected from 60 children, including 32 healthy controls, 9 surgical controls (in whom no CRT was performed, but 2 patients received chemotherapy), and 19 CRT patients. Each patient received 1 to 4 scans (average, 2.4 scans) with an average scan age of 11.2 years. The 19 CRT patients were divided into 2 groups based on age at diagnosis, consisting of those 7 years of age and younger (7−) and 8 years of age and older (8+; n = 11 and 8 patients, respectively). Figure 1a and Supplementary Table 1 (available online at

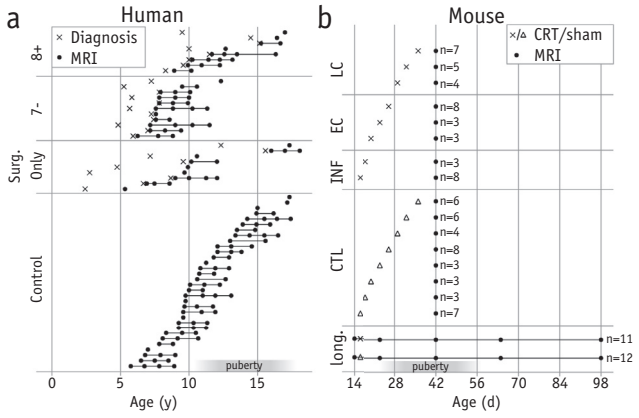

Fig. 1. Timelines for human and mouse imaging studies. (a) Each row shows a subject in the Control, Surgical Control, diagnosis at 7 and under (7−), or diagnosis at 8 and over (8+) group. Imaging time points (MRI) are shown with black dots, and diagnosis age is shown with an x. Lines connect scans collected longitudinally. (b) An equivalent timeline for the mouse experiments is also shown. A longitudinal study (bottom lines) was conducted in vivo with cranial radiation therapy (CRT) or sham at postnatal day 16 (P16). Additionally, a series of groups were evaluated ex vivo after treatment at different ages. The latter were grouped into infancy (INF), early-childhood (EC), and late childhood (LC). *Abbreviations:* d = days; y = years.

www.redjournal.com) provide further information. The majority of CRT patients (14 of 19) received a total craniospinal dose of 23.4 Gy; 1 patient received 30.6 Gy and 4 received 36 Gy. Total dose to the posterior fossa was boosted to 54 Gy (4 patients), 55.8 Gy (14 patients), or 59.4 Gy (1 patient). Analyses of single time point data and other image contrasts (ie, diffusion images) have been reported previously for a subset of the patients and controls used in the present cohort (12, 25, 26).

From image data, we computed total and lobe-specific WM and GM volumes, cortical thicknesses, and hippocampal volumes. MRI results were fitted with a linear mixed effects model with a coefficient for age at scanning and a coefficient representing a constant offset for each of the 7− and 8+ CRT groups. Variability among patients was accounted for with a subject-specific random intercept term. In each case, the significance of an additional coefficient for time since diagnosis was also tested. Supplementary materials (available online at www.redjournal.com) provide additional details of the imaging and analysis methods (25, 27-36). Where multiple statistical comparisons were performed, significance was tested after adjustment of the *P* value by using the false discovery rate (FDR; referring to the adjusted value as the Q value).

Mouse experiments

We compared human results to observations in a mouse model of CRT (22, 23). All mouse experiments were approved by the Toronto Centre for Phenogenomics Animal Care Committee. Acquisition of image data was previously described (23). Briefly, C57BL/6J mice were irradiated with 0 or 7 Gy at a single time point between postnatal day 16 (P16) and P36. Assuming a linear quadratic model (with an α/β ratio of 2 Gy), this dose is considered equivalent to ~16 Gy delivered in 2-Gy fractions. Due to the rapid rate of mouse development and to limit effects from frequent handling, a fractionated delivery was not used. To facilitate comparison with patient data, treatment ages for mice were combined into infancy (INF) (P16-P18), early childhood (EC) (P20-P26), and late childhood (LC) (P29-P36) treatment groups. From the MR images, we computed WM and GM volumes, cortical thicknesses, and brain structure volumes based on an existing atlas (which included hippocampal volume) (40). In vivo data were fitted with a linear mixed effects model, with mouse-specific random intercept coefficients and fixed coefficients representing normal development by a spline and a treatment-dependent deviation with coefficients for a constant offset and a slope linear in age. Ex vivo data were fitted with a simple linear model, fitting a spline in treatment age to the deviation from the mean control volume. Additional experimental details can be found in Figure 1b and supplementary materials (available online at www.redjournal.com) (37-41).

Results

WM volume is decreased following pediatric CRT

In both the 7− and 8 + CRT patient groups, we observed a smaller total (supratentorial) WM volume than in controls ($P<.01$ and $P<.05$, respectively) (Fig. 2a, b). WM volumes in surgical controls did not differ from healthy controls ($P=.87$) and were grouped together for all analyses. Frontal, parietal, temporal, and occipital lobe WM volumes were significantly smaller in the 7− CRT group on both sides of the brain ($Q < .05$) (Fig. 2e, f). The 8 + CRT group also showed decreased volumes ($Q < .05$), except in the left temporal and left occipital lobes ($Q=.07$ and .17, respectively). Time since diagnosis did not contribute to a model of the WM volume results, suggesting that the WM volume was present prior to the first post-treatment scans.

Substantiating observations of WM in humans, radiation-treated mice showed decreased WM volume. The volume decrease occurred early after CRT and was followed by a growth rate comparable to that in untreated mice, resulting in a persistent volume deficit (Fig. 2c). Treatment at later ages resulted in more normal total WM volumes (Fig. 2d), with no differences apparent when CRT occurred in the LC stages.

Changes in cortical GM after pediatric CRT

Total GM volume in humans was not substantially different between control and CRT groups (Fig. 3a). More detailed

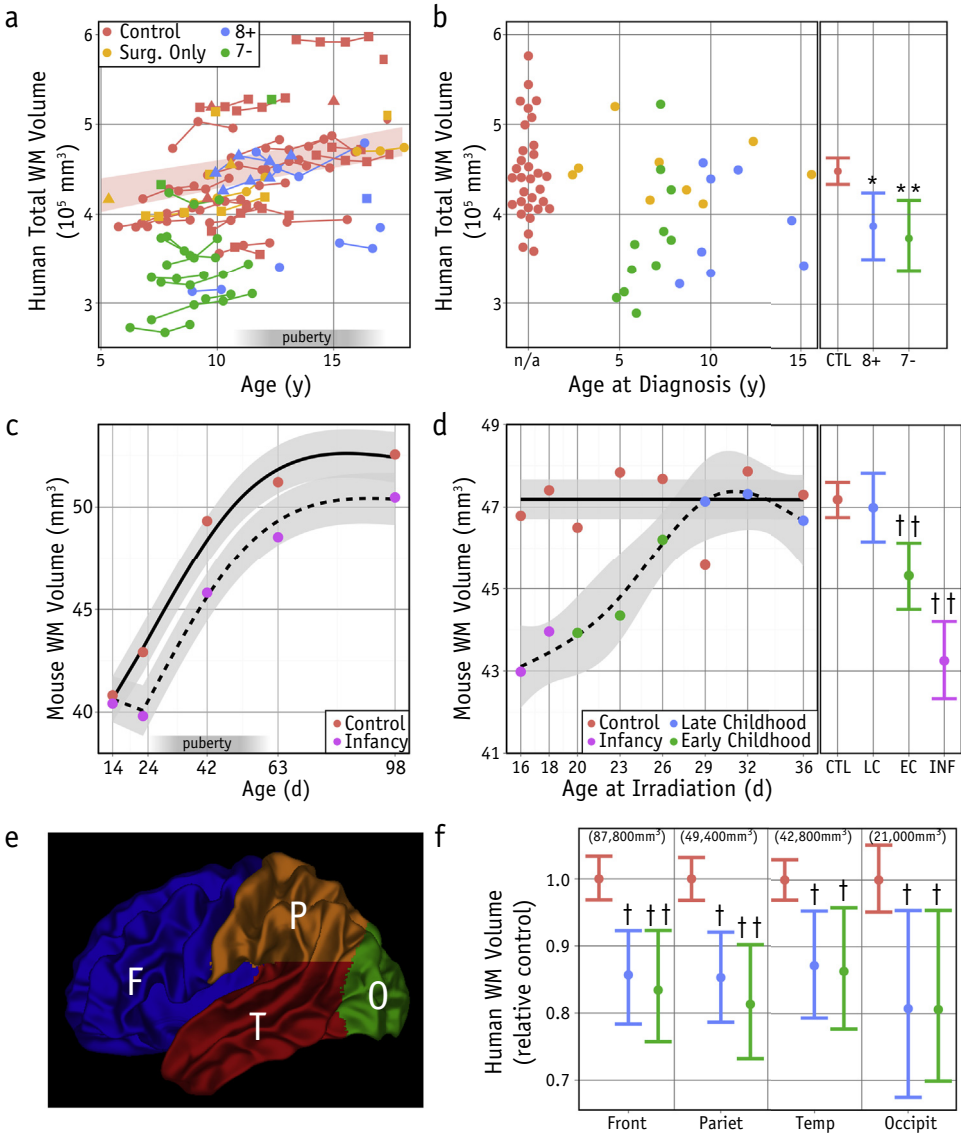

Fig. 2. White matter volume is decreased after cranial radiation therapy (CRT). Total white matter (WM) volume was computed for all patient images (a). The fit of the linear mixed effects model (shaded red for control [CTL] group) was used to compute a volume for each patient, normalized to 11.2 years (y) of age. (b) This normalized volume is plotted against age at diagnosis. Volume is significantly decreased in both the 8+ and 7− groups ($P<.05$ and $P<.01$, respectively). CRT in mice provided more comprehensive coverage of treatment and imaging ages. (c, d) Each point represents the group mean for all mice for that time point, with pooling into infancy (INF), early childhood (EC), and late childhood (LC), indicated by color coding (d). (c) In mice, a WM volume decrease of ∼7% was observed by the first imaging time point after treatment ($P<.0001$), which persisted to adulthood. (d) The degree of deficit decreased when treatment was delayed to later ages, with INF (Q = 3e-5) and EC (Q = .003) but not LC groups showing significant differences. (e) Separation of human WM into frontal (F), parietal (P), occipital (O), and temporal (T) lobes allowed comparison of lobe volumes. (f) Both of the patient groups showed significant volume differences (Q < .05 for 8+ and Q < .01 for 7−, right side shown). Occipital and temporal lobe WM volume differences did not reach significance on the left side (Q = .17 and .07 respectively). Shaded areas and error bars show 95% confidence intervals (*$P<.05$, **$P<.01$; †Q < .1, ††Q < .01). A color version of this figure is available at www.redjournal.org.

analysis of the cortical GM revealed that, in the 7− CRT group, average cortical thickness was slightly increased in the frontal, occipital, and temporal lobes (Q < .1) but not significantly in the parietal lobe (Fig. 3b). No significant differences in cortical thicknesses were observed in the 8 + group.

Total GM volume in treated mouse brains showed a modest decrease relative to that of controls (Fig. 3c), which persisted unchanged throughout development. Average measurements of mouse cortical thicknesses across each lobe revealed only a small increase in the occipital lobe

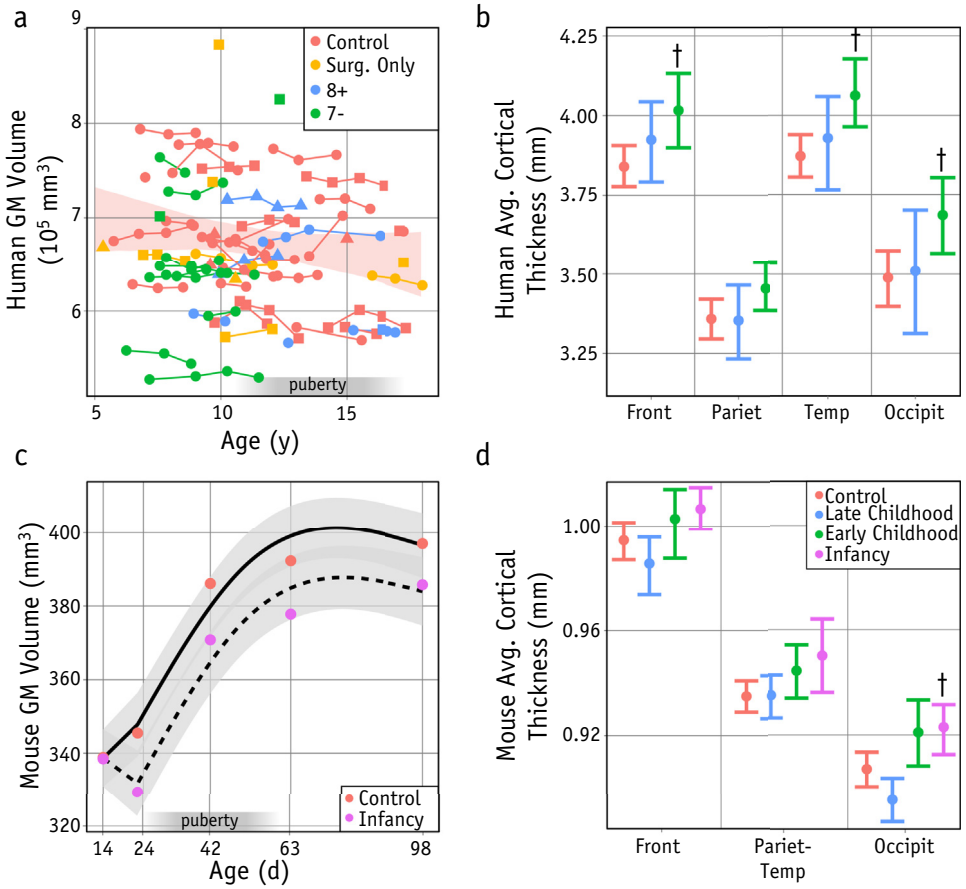

Fig. 3. Cortical gray matter (GM) is altered after cranial radiation therapy (CRT). Total GM volume was computed for all patient images (a) and was not significantly different between treated and untreated groups. (b) Analysis of cortical thickness showed increased thickness in the 7− group in the frontal, occipital, and temporal lobes (Q < .1) but not in the parietal lobe. (c) Total gray matter over time after CRT at P16 in the mouse is shown. An initial 5% drop is observed (P = .0002), but subsequent growth over time was not different from that of controls. (d) Measurements of cortical thickness in the frontal, parietotemporal, and occipital lobes are shown. An increase in thickness was observed only in the occipital lobe after treatment in infancy (Q = .03) but not significantly in the frontal and parietotemporal lobes (Q = .14 and .29, respectively). Additional cortical thickness results are shown in Fig. 4 (†Q < .1).

(Q = .03) (Fig. 3d). However, more localized analysis showed that the ventral orbital cortex was thicker in treated mice (Fig. 4). Thickness differences appeared shortly after treatment and grew over time (largely due to thinning in controls after ∼ P42) (Fig. 4b). This change in cortical thickness was present in treatments at INF and EC (Q = 8e-5 and .04, respectively), but was eliminated when treatment was delayed to LC (Fig. 4c).

We also evaluated cortical surface area and volume in humans and mice (Fig. 5). In human data, we detected no statistical differences between these parameters after multiple comparison correction, although there may be a trend toward decreased surface area. Similar measurements in the mouse showed a cortical surface area decrease only in the INF group (Q = .003, .004, and .003 for frontal, parietotemporal, and occipital lobes, respectively) (Fig. 5c) and no differences in total cortical volume. In human data, we also computed the gyrification index (42), which showed no differences, and the ratio of the square root of the surface area to the thickness (a cortical aspect ratio, with larger values representing thinner sheets with larger areas). This measure was significantly reduced in the frontal, occipital, and temporal lobes (Q < .05) on both sides of the brain in the 7- group and in the parietal lobes to a lesser degree (Q = .16 and Q = .04 for left and right sides, respectively).

Decreased hippocampal volume after CRT

We further investigated GM by assessing total hippocampal volume, which did not show a significant dependence on treatment group (Fig. 6a, b). However, addition of time since CRT to the model for patient groups showed a significant negative term (P<.01), indicating a decreasing hippocampal volume post treatment in CRT patients (Fig. 6c). Relative to the hippocampal volume of controls (which was modestly increasing at a rate of 28 mm^3/year;

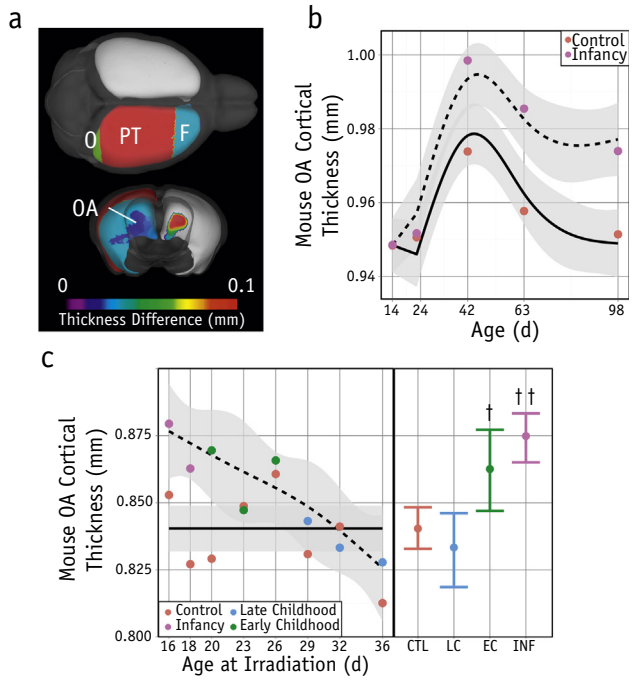

Fig. 4. Orbital areas of mouse cortex showed increased thickness. (a) Segmentation of the orbital area (OA) in the mouse brain is shown, along with the frontal (F), parieto-temporal (PT), and occipital (O) lobes. On the right side of the lower panel in (a), a map of significantly different thickness measurements due to cranial radiation therapy (CRT) at P16 is shown, where $Q < .01$ for each vertex of the surface (otherwise colored white). (b) Average cortical thickness over the OA is shown longitudinally, indicating an increasing thickness relative to that of controls (CTL) to early adulthood. (c) OA thickness is shown after CRT at different ages. Significant differences after CRT were detected after treatment in infancy (INF) ($Q = 8e\text{-}5$) and early childhood (EC) ($Q = .04$) but not late childhood (LC). Error bars and shaded areas show 95% confidence intervals (†$Q < .1$, ††$Q < .01$).

$P < .02$), this amounted to a relative decrease in volume of 99 mm^3/year (or ∼3% volume decrease relative to controls).

In the mouse model, hippocampal volume showed an early volume decrease after CRT in the INF group (Fig. 6d) but not in the EC or LC group (Fig. 6e). Like much of the mouse brain and unlike the human hippocampus, this difference persisted without significant change (Fig. 6f). We also evaluated the volume time course of the olfactory bulb, another structure with significant neural progenitor cell input. It showed an immediate volume decrease post-CRT (Fig. 6g) that depended on age at treatment (Fig. 6h). In addition, the olfactory bulb showed a progressive volume deficit resulting from a decreased growth rate relative to controls (Fig. 6i, INF), more reminiscent of the growth changes observed in the human hippocampus.

Discussion

The results we observed indicate significant changes in both WM and GM after CRT. The WM changes were expected from previous reports (10, 15, 43). Supplementing the human observations with experiments in mice supported the possibility that the WM volume loss occurs very early after CRT and then does not recover during development. This observation may indicate that normalization of late effects related to WM loss would require an early intervention and/or a strategy for protecting WM during CRT.

We observed cortical and hippocampal GM alterations. Normal cortical development includes an early growth and a subsequent volume decrease with a peak thickness at 7 to 11 years of age (44-46). Thickness changes through adolescence (as seen on MRI) are normally influenced by synaptic pruning (47) and underlying white matter myelination (44). However, as most of the initial scans had been acquired within a year or two of treatment, the cortical differences we observed appeared to develop relatively quickly, which might suggest inflammation, gliosis, or other abnormal processes initiated by CRT. Moreover, it seems likely that the changes in cortical thickness and WM volume are related (48), but which is the most important in manifesting late effects still needs to be determined. In addition, we noted that the changes in average cortical thickness that we observed after CRT were opposite to those reported previously (49), indicating need for further verification.

We also observed loss of ∼2% per year in the total volume of hippocampus in CRT patients (vs ∼1%/year growth in controls). In the adult human hippocampus, there is an estimated 3.5% per year and 1.75% per year turnover in non-neuronal and neuronal cell populations, respectively (in which an estimated 50% and 33%, respectively, of total cell populations are affected) (50). Decreasing hippocampal volume after CRT may result from normal cell loss combined with a reduced capacity to generate new cells for replacement and ongoing growth. In the mouse, we observed an early volume decrease of ∼5% after CRT, with no change in growth rate. The fact that we did not detect an early volume decrease in the human hippocampus may be a simple question of sensitivity (given the standard deviation of ∼10% in human hippocampal volumes, we had only enough statistical power to detect differences of ∼10%, assuming a power of 0.8 and a significance of .05). Differences in post-treatment hippocampal growth rates between species, however, are likely a real effect, and may be due to species differences in the rate and population of cells subject to turnover. Relative to the rate of cell replacement in humans, the mouse has a limited number of cells being replaced at a faster rate (eg, ∼10% of mouse hippocampal neurons are replaced in ∼4 months [51]). Like the human hippocampus, the mouse olfactory bulbs exhibited a progressive volume

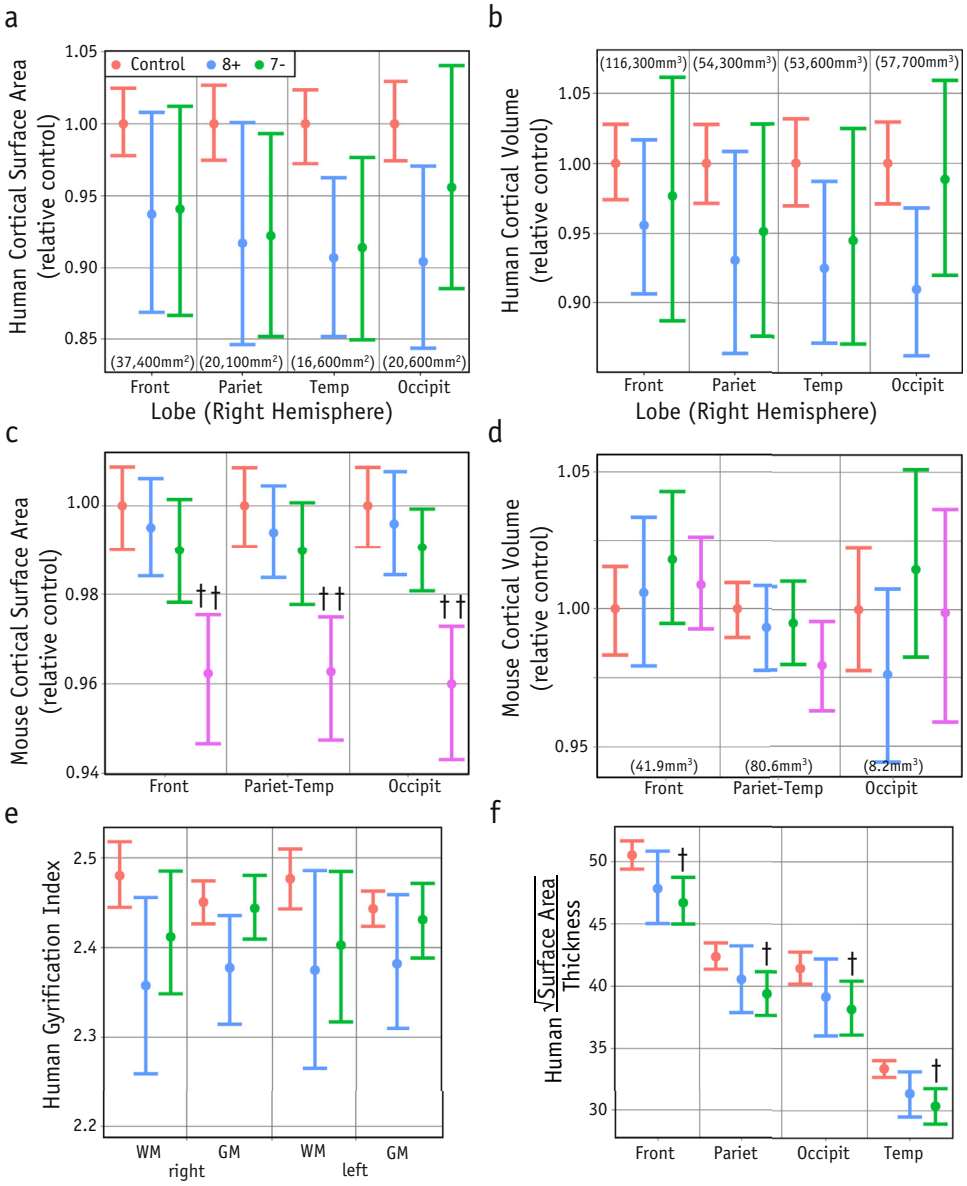

Fig. 5. Additional cortical geometry measurements. Measurements of total cortical surface area (a) and cortical volume (b) were made for each lobe (right side shown unless indicated). No differences reached significance. Similar measurements in the mouse (c, d) showed a decrease in cortical surface areas of ∼4% after treatment in infancy (Q = .003, .004 and .003 for frontal, parietotemporal and occipital lobes) but not at later treatment ages. In humans, the gyrification index (e) also showed no significant differences at the white matter [WM] or the gray matter [GM]. Comparisons of the root of the surface areas over the thickness (an aspect ratio that is large for thin sheets) showed that all lobes were different in the 7− patient group (Q < .05) (f). Error bars in all cases show 95% confidence intervals (†Q < .1, ††Q < .01).

deficit after CRT. Although the granule cell layer of the mouse olfactory bulb has properties similar to those of the hippocampus, the glomerular layer turns over at the rate of ∼40%/year (51). These differences in cellular kinetics may determine the species-specific changes in growth after CRT.

Overall, mouse model data showed substantial parallels to those of the humans in WM volume and GM cortical outcome measurements (although the latter were more localized). Nonetheless, we noted that the mouse experiments could not entirely mimic the human case and that treatment differences between species might have affected outcomes. First, the short developmental time course in mice is incompatible with the fractionated doses used in patients, which in the mouse would span from infancy well into puberty if used unaltered. As an alternative, we delivered CRT to mice in a single fraction that provides a temporally localized radiation insult and allows brain development to progress undisturbed thereafter. Different doses or fraction schedules are likely to alter some aspects

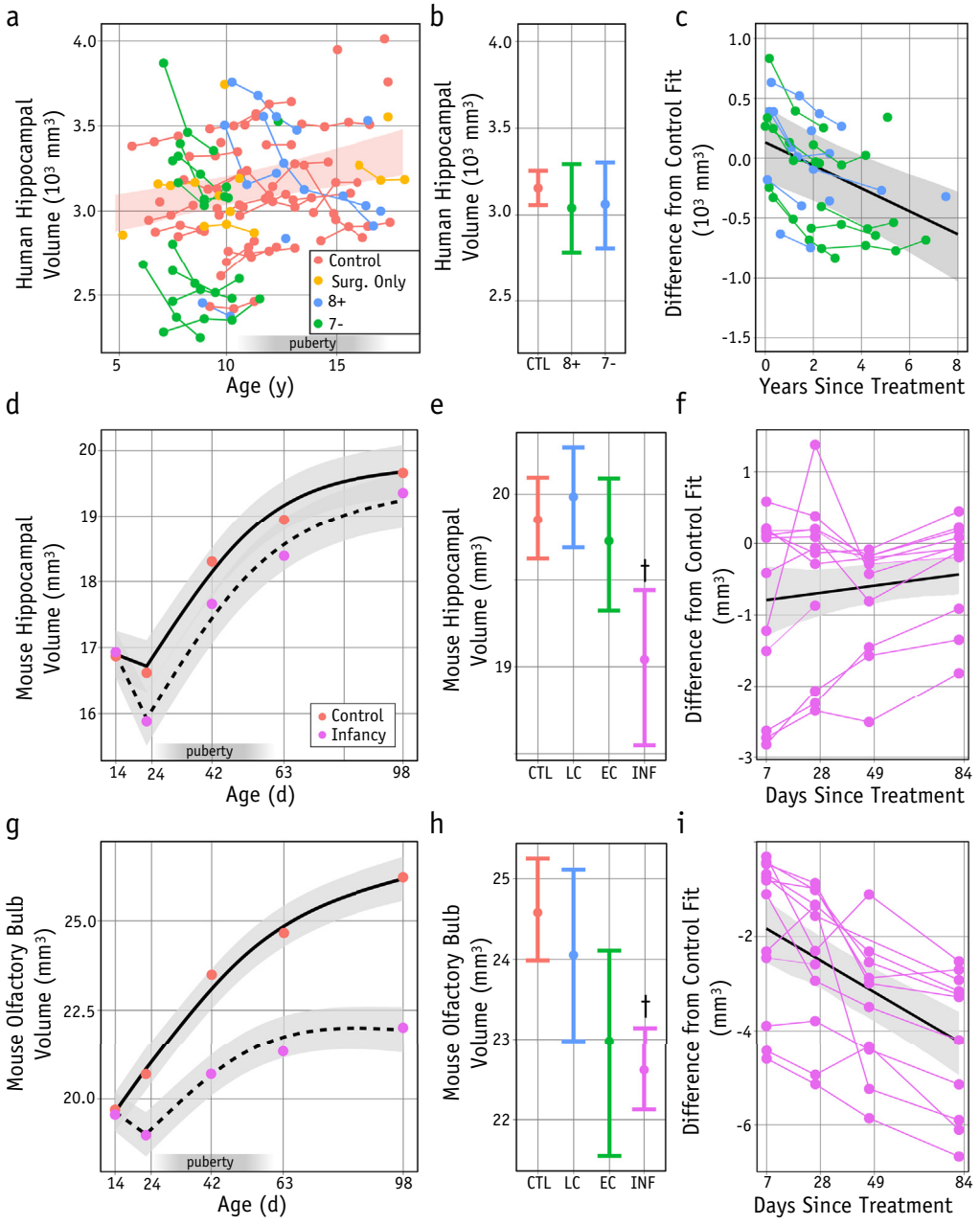

Fig. 6. Hippocampal volume and growth after cranial radiation therapy (CRT). Total hippocampal volume, shown for all patient images (a), showed no significant differences between controls (CTL) and either of the patient groups. This is viewed after normalization to 11.2 years (y) (b). Hippocampal volume was observed to grow in CTL (95% confidence intervals in red for fit line [a]). In the treated goups, however, a decreasing volume with time since treatment was observed. (c) Deviation from the control fit is shown for each patient, with time since treatment on the horizontal axis for both the 7− and the 8+ groups. The black line shows the fit (common to the 7− and 8+ groups) with 95% confidence intervals. In the mouse, hippocampal volume showed an initial volume decrease ($Q < .05$) after CRT at P16 (d), but then growth was normal, with no differences from that of controls (f). Hippocampal volume comparisons between groups of mice was significant only in the infant (INF) treatment group ($Q = .02$) (e). The olfactory bulb, another region of active neurogenesis in the mouse, also showed an initial volume decrease ($Q < .05$) (g). Significant group differences were seen only in the INF treatment group (h) ($Q = .0004$). EC = early childhood; LC = late childhood. In the olfactory bulb, growth after treatment was also altered (-0.03 mm^3/day relative to that of controls) (i). (†$Q < .1$). A color version of this figure is available at www.redjournal.org.

of outcome. Second, we delivered a uniform dose across the whole brain in the mice, although patients received a spatially heterogeneous dose with a boost to the posterior fossa. More recent tools for focal irradiation in the mouse would allow more accurate replication of such a distribution (52). Third, we noted that the anatomy of the mouse

brain is quite different, with little white matter and a flat cortical geometry, and that the mice did not have pre-existing tumors at treatment. The latter is a considerable advantage of the mouse model because the effect of CRT can be separated from cancer effects in a way not possible in patients. Despite these human-mouse differences, our MRI data indicate significant parallels between species after CRT.

Conclusions

In conclusion, this study confirmed significant loss of WM after CRT in pediatric patients and also revealed an increase in cortical thickness and a decreasing hippocampal volume. A mouse model in which CRT is provided in a single dose, in the absence of ancillary treatment or disease, mimicked many of these features and suggests some changes occur very early after treatment. Further experiments in mice will permit testing of late effect interventions or possible treatment modifications. Results also highlighted some species differences that necessitate careful interpretation when translating to patients.

References

1. Ris MD, Packer R, Goldwein J, et al. Intellectual outcome after reduced-dose radiation therapy plus adjuvant chemotherapy for medulloblastoma: A Children's Cancer Group study. *J Clin Oncol* 2001; 19:3470-3476.
2. Mitby PA, Robison LL, Whitton JA, et al. Utilization of special education services and educational attainment among long-term survivors of childhood cancer: A report from the Childhood Cancer Survivor Study. *Cancer* 2003;97:1115-1126.
3. Nathan PC, Patel SK, Dilley K, et al. Guidelines for identification of, advocacy for, and intervention in neurocognitive problems in survivors of childhood cancer: A report from the Children's Oncology Group. *Arch Pediatr Adolesc Med* 2007;161:798-806.
4. Anderson DM, Rennie KM, Ziegler RS, et al. Medical and neurocognitive late effects among survivors of childhood central nervous system tumors. *Cancer* 2001;92:2709-2719.
5. Schultz KA, Ness KK, Whitton J, et al. Behavioral and social outcomes in adolescent survivors of childhood cancer: A report from the childhood cancer survivor study. *J Clin Oncol* 2007;25:3649-3656.
6. Palmer SL, Goloubeva O, Reddick WE, et al. Patterns of intellectual development among survivors of pediatric medulloblastoma: A longitudinal analysis. *J Clin Oncol* 2001;19:2302-2308.
7. Meyers CA, Smith JA, Bezjak A, et al. Neurocognitive function and progression in patients with brain metastases treated with whole-brain radiation and motexafin gadolinium: Results of a randomized phase III trial. *J Clin Oncol* 2004;22:157-165.
8. Spiegler BJ, Bouffet E, Greenberg ML, et al. Change in neurocognitive functioning after treatment with cranial radiation in childhood. *J Clin Oncol* 2004;22:706-713.
9. Ellenberg L, Liu Q, Gioia G, et al. Neurocognitive status in long-term survivors of childhood CNS malignancies: A report from the Childhood Cancer Survivor Study. *Neuropsychology* 2009;23:705-717.
10. Mulhern RK, Reddick WE, Palmer SL, et al. Neurocognitive deficits in medulloblastoma survivors and white matter loss. *Ann Neurol* 1999;46:834-841.
11. Rueckriegel SM, Driever PH, Blankenburg F, et al. Differences in supratentorial damage of white matter in pediatric survivors of posterior fossa tumors with and without adjuvant treatment as detected by magnetic resonance diffusion tensor imaging. *Int J Radiat Oncol Biol Phys* 2010;76:859-866.
12. Riggs L, Bouffet E, Laughlin S, et al. Changes to memory structures in children treated for posterior fossa tumors. *J Int Neuropsychol Soc* 2014;20:168-180.
13. Reddick WE, White HA, Glass JO, et al. Developmental model relating white matter volume to neurocognitive deficits in pediatric brain tumor survivors. *Cancer* 2003;97:2512-2519.
14. Khong PL, Leung LH, Fung AS, et al. White matter anisotropy in post-treatment childhood cancer survivors: Preliminary evidence of association with neurocognitive function. *J Clin Oncol* 2006;24: 884-890.
15. Mabbott DJ, Noseworthy MD, Bouffet E, et al. Diffusion tensor imaging of white matter after cranial radiation in children for medulloblastoma: correlation with IQ. *Neuro Oncol* 2006;8:244-252.
16. Landier W, Bhatia S. Cancer survivorship: A pediatric perspective. *Oncologist* 2008;13:1181-1192.
17. Rola R, Raber J, Rizk A, et al. Radiation-induced impairment of hippocampal neurogenesis is associated with cognitive deficits in young mice. *Exp Neurol* 2004;188:316-330.
18. Rao AA, Ye H, Decker PA, et al. Therapeutic doses of cranial irradiation induce hippocampus-dependent cognitive deficits in young mice. *J Neurooncol* 2011;105:191-198.
19. Karlsson N, Kalm M, Nilsson MK, et al. Learning and activity after irradiation of the young mouse brain analyzed in adulthood using unbiased monitoring in a home cage environment. *Radiat Res* 2011; 175:336-346.
20. Nieman BJ, Lerch JP, Bock NA, et al. Mouse behavioral mutants have neuroimaging abnormalities. *Hum Brain Mapp* 2007;28:567-575.
21. Ellegood J, Babineau BA, Henkelman RM, et al. Neuroanatomical analysis of the BTBR mouse model of autism using magnetic resonance imaging and diffusion tensor imaging. *Neuroimage* 2013;70: 288-300.
22. Gazdzinski LM, Cormier K, Lu FG, et al. Radiation-induced alterations in mouse brain development characterized by magnetic resonance imaging. *Int J Radiat Oncol Biol Phys* 2012;84:e631-e638.
23. de Guzman AE, Gazdzinski LM, Alsop RJ, et al. Treatment age, dose and sex determine neuroanatomical outcome in irradiated juvenile mice. *Radiat Res* 2015;183:541-549.
24. Grill J, Renaux VK, Bulteau C, et al. Long-term intellectual outcome in children with posterior fossa tumors according to radiation doses and volumes. *Int J Radiat Oncol Biol Phys* 1999;45:137-145.
25. Law N, Bouffet E, Laughlin S, et al. Cerebello-thalamo-cerebral connections in pediatric brain tumor patients: impact on working memory. *Neuroimage* 2011;56:2238-2248.
26. Law N, Greenberg M, Bouffet E, et al. Clinical and neuroanatomical predictors of cerebellar mutism syndrome. *Neuro Oncol* 2012;14: 1294-1303.
27. Zijdenbos AP, Forghani R, Evans AC. Automatic "pipeline" analysis of 3-D MRI data for clinical trials: Application to multiple sclerosis. *IEEE Trans Med Imaging* 2002;21:1280-1291.
28. Collins DL, Neelin P, Peters TM, et al. Automatic 3D intersubject registration of MR volumetric data in standardized Talairach space. *J Comput Assist Tomogr* 1994;18:192-205.
29. Sled JG, Zijdenbos AP, Evans AC. A nonparametric method for automatic correction of intensity nonuniformity in MRI data. *IEEE Trans Med Imaging* 1998;17:87-97.
30. Zhang Y, Brady M, Smith S. Segmentation of brain MR images through a hidden Markov random field model and the expectation-maximization algorithm. *IEEE Trans Med Imaging* 2001;20:45-57.
31. Kim JS, Singh V, Lee JK, et al. Automated 3-D extraction and evaluation of the inner and outer cortical surfaces using a Laplacian map and partial volume effect classification. *Neuroimage* 2005;27: 210-221.

32. Lyttelton O, Boucher M, Robbins S, et al. An unbiased iterative group registration template for cortical surface analysis. *Neuroimage* 2007;34:1535-1544.
33. Lerch JP, Evans AC. Cortical thickness analysis examined through power analysis and a population simulation. *Neuroimage* 2005;24: 163-173.
34. Chakravarty MM, Steadman P, van Eede MC, et al. Performing label-fusion-based segmentation using multiple automatically generated templates. *Hum Brain Mapp* 2013;34:2635-2654.
35. Winterburn JL, Pruessner JC, Chavez S, et al. A novel in vivo atlas of human hippocampal subfields using high-resolution 3 T magnetic resonance imaging. *Neuroimage* 2013;74:254-265.
36. Pipitone J, Park MT, Winterburn J, et al. Multi-atlas segmentation of the whole hippocampus and subfields using multiple automatically generated templates. *Neuroimage* 2014;101:494-512.
37. Lerch JP, Gazdzinski L, Germann J, et al. Wanted dead or alive? The tradeoff between in-vivo versus ex-vivo MR brain imaging in the mouse. *Front Neuroinform* 2012;6:6.
38. Nieman BJ, Flenniken AM, Adamson SL, et al. Anatomical phenotyping in the brain and skull of a mutant mouse by magnetic resonance imaging and computed tomography. *Physiol Genomics* 2006; 24:154-162.
39. Lerch JP, Yiu AP, Martinez-Canabal A, et al. Maze training in mice induces MRI-detectable brain shape changes specific to the type of learning. *Neuroimage* 2011;54:2086-2095.
40. Dorr AE, Lerch JP, Spring S, et al. High resolution three-dimensional brain atlas using an average magnetic resonance image of 40 adult C57Bl/6J mice. *Neuroimage* 2008;42:60-69.
41. Lerch JP, Carroll JB, Spring S, et al. Automated deformation analysis in the YAC128 Huntington disease mouse model. *Neuroimage* 2008; 39:32-39.
42. Zilles K, Armstrong E, Schleicher A, et al. The human pattern of gyrification in the cerebral cortex. *Anat Embryol (Berl)* 1988;179: 173-179.
43. Reddick WE, Shan ZY, Glass JO, et al. Smaller white-matter volumes are associated with larger deficits in attention and learning among long-term survivors of acute lymphoblastic leukemia. *Cancer* 2006;106:941-949.
44. Courchesne E, Chisum HJ, Townsend J, et al. Normal brain development and aging: Quantitative analysis at in vivo MR imaging in healthy volunteers. *Radiology* 2000;216:672-682.
45. Gogtay N, Giedd JN, Lusk L, et al. Dynamic mapping of human cortical development during childhood through early adulthood. *Proc Natl Acad Sci U S A* 2004;101:8174-8179.
46. Shaw P, Kabani NJ, Lerch JP, et al. Neurodevelopmental trajectories of the human cerebral cortex. *J Neurosci* 2008;28:3586-3594.
47. Webb SJ, Monk CS, Nelson CA. Mechanisms of postnatal neurobiological development: Implications for human development. *Dev Neuropsychol* 2001;19:147-171.
48. Alexander-Bloch A, Giedd JN, Bullmore E. Imaging structural covariance between human brain regions. *Nat Rev Neurosci* 2013;14: 322-336.
49. Liu AK, Marcus KJ, Fischl B, et al. Changes in cerebral cortex of children treated for medulloblastoma. *Int J Radiat Oncol Biol Phys* 2007;68:992-998.
50. Spalding KL, Bergmann O, Alkass K, et al. Dynamics of hippocampal neurogenesis in adult humans. *Cell* 2013;153:1219-1227.
51. Ninkovic J, Mori T, Götz M. Distinct modes of neuron addition in adult mouse neurogenesis. *J Neurosci* 2007;27:10906-10911.
52. Clarkson R, Lindsay PE, Ansell S, et al. Characterization of image quality and image-guidance performance of a preclinical microirradiator. *Med Phys* 2011;38:845-856.